CHAPTER – VIII

QUANTUM CHEMISTRY CALCULATIONS OF 4-PHENOXYPHTHALONITRILE(4PPN) DYE SENSITIZER FOR SOLAR CELLS

CHAPTER – VIII

Quantum Chemistry Calculations of

4-Phenoxyphthalonitrile(4PPN) Dye Sensitizer for Solar Cells

8.1 Introduction to 4PPN

In a Dye Sensitized Solar Cell (DSSC) the process of electron transfer between adsorbed dye molecule and semiconductor substrates is very important. In this chapter studies have mainly focused on the properties relevant for electron transfer. For this a phthalonitrile dye sensitizer 4-Phenoxyphthalonitrile (4PPN) (CAS Number: 38791-62-7) is selected for our study. This metal free dye has linear formula : C6H5OC6H3-1,2-(CN)2 and its molecular weight is 220.23 [g/mol]. The performance of this metal free dye 4PPN that can be used in DSSC is studied and results are discussed.

8.2 Experimental Details for 4PPN

The compound 4PPN was obtained and taken with a stated purity of greater than 99% and it was used as such without further purification. The FT-Raman spectrum of 4PPN has been recorded using 1064 nm line of Nd:YAG laser as excitation wavelength in the region 50-3500 cm^{-1} on a Brucker model IFS 66 V spectrophotometer. The FT-IR spectrum of this compound was recorded in the region 400-4000 cm^{-1} on IFS 66 V spectrophotometer using KBr pellet technique. The spectrum was recorded at room temperature, with scanning speed of 30 cm^{-1} and the spectral resolution of 2.0 cm^{-1}.

8.3 Computational methods for 4PPN

The computations of the geometries, electronic structures, polarizabilities and hyperpolarizabilities, as well as electronic absorption spectrum for dye sensitizer 4PPN was done using Hartree-Fock (HF) and Density Functional Theory (DFT) with

Gaussian03 package [1]. The DFT was treated with hybrid functional Becke's three parameter and the Lee-Yang-Parr potential (B3LYP) [2-4], and all calculations were performed without any symmetry constraints by using polarized split-valence 6-311G++(d,p) basis sets. The NBO analysis were performed using Restricted Hartree Fock (RHF) with the 6-311++G(d,p) basis sets. The electronic absorption spectrum requires calculation of the allowed excitations and oscillator strengths. These calculations were done using TD-DFT with the Perdew-Burke-Ernzerhof exchange-correlation functional (PBE1PBE) applied to 6-311++G(d,p) basis set in vacuum and acetonitrile solution, and the non-equilibrium version of the Polarizable Continuum Model (PCM) [5,6] was adopted for calculating the solvent effects

8.4 Results and discussion

8.4.1 The geometric structure of 4PPN

The optimized geometry of the 4PPN is shown in Figure 8.1, and the bond lengths, bond angles and dihedral angles are listed in Table 8.1. From the theoretical values we can find the optimized bond lengths, bond angles and dihedral angles. The optimized bond lengths of C8-C16 and C9-C17 is 1.4307and 1.4270Å respectively at B3LYP/6-311G++ (d,p) and also well matched with HF/6-311G++ (d,p).

8.4.2 Electronic structures and charges of 4PPN

Natural Bond Orbital (NBO) analysis was performed in order to analyze the charge populations of the dye 4PPN. Charge distributions in C, N and H atoms were observed because of the different electro-negativity, the electrons transferred from C atoms to C, N atoms, C atoms to H. The natural charges of different groups are the sum of every atomic natural charge in the group. These data indicate that the cyanine and amide groups are acceptors, while the acetic groups are donors, and the charges were transferred through chemical bonds. The frontier molecular orbitals (MO) energies and

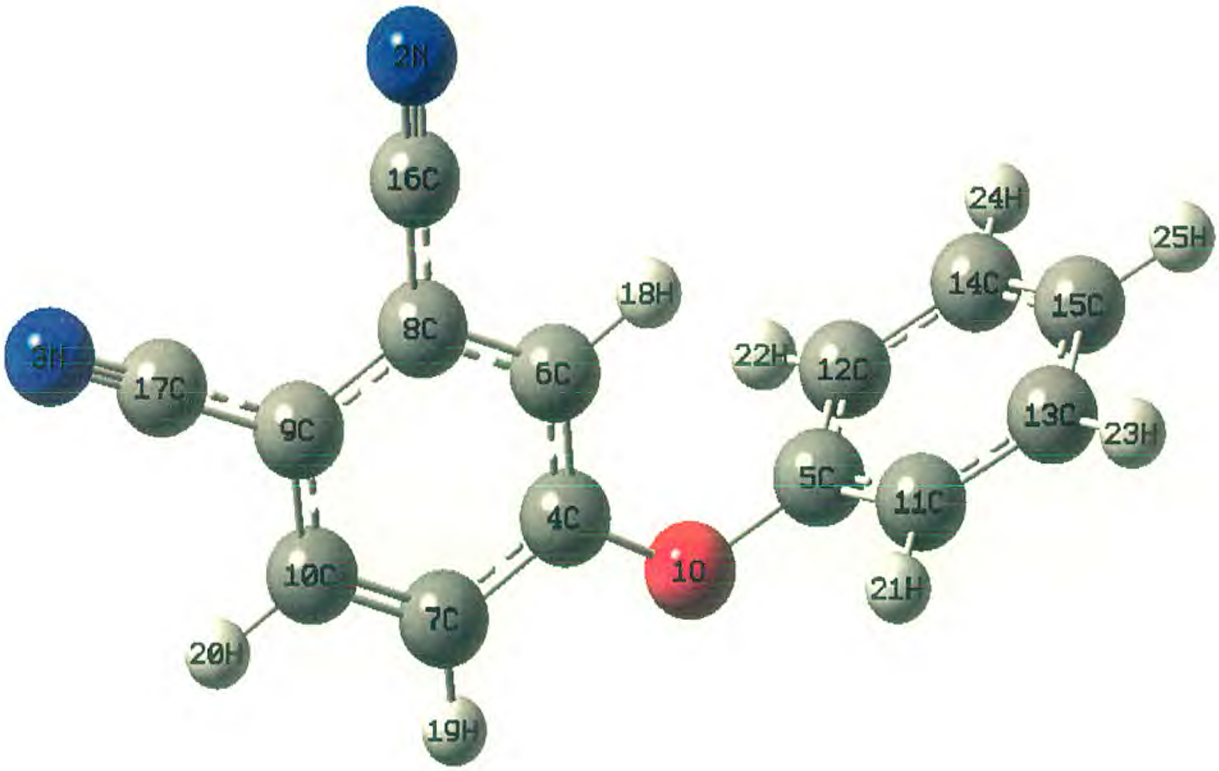

Figure 8.1 Optimized geometrical structure of dye 4PPN

Table 8.1 Bond lengths (in Å), bond angles (in degree) and dihedral angles (in degree) of the dye 4PPN

Parameters	HF/6-311++G(d,p)	B3LYP/6-311++G(d,p)
Bond length(Å)		
O1-C4	1.3447	1.3615
O1-C5	1.3770	1.3975
N2-C16	1.1293	1.1545
N3-C17	1.1299	1.1551
C4-C6	1.3847	1.3946
C4-C7	1.3906	1.4003
C5-C11	1.3805	1.3902
C5-C12	1.3805	1.3902
C6-C8	1.3878	1.3987
C6-H18	1.0711	1.0807
C7-C10	1.3742	1.3826
C7-H19	1.0733	1.0825
C8-C9	1.3906	1.4104
C8-C16	1.4432	1.4307
C9-C10	1.3916	1.4031
C9-C17	1.4391	1.4270
C10-H20	1.0736	1.0825
C11-C13	1.3849	1.3934
C11-H21	1.0746	1.0833
C12-C14	1.3849	1.3934
C12-H22	1.0746	1.0833
C13-C15	1.3850	1.3938
C13-H23	1.0749	1.0837
C14-C15	1.3850	1.3938
C14-H24	1.0749	1.0837
C15-H25	1.0747	1.0835
Bond Angle(°)		
C4-O1-C5	121.2	120.0163
O1-C4-C6	124.1	123.9884

Table 8.1 (Contd..)Bond lengths (in Å), bond angles (in degree) and dihedral angles (in degree) of the dye 4PPN

Parameters	HF/6-311++G(d,p)	B3LYP/6-311++G(d,p)
Bond Angle(°)		
O1-C4-C7	115.7	115.8781
C6-C4-C7	120.0	120.1335
O1-C5-C11	119.2	119.1878
O1-C5-C12	119.2	119.1795
C11-C5-C12	121.3	121.5417
C4-C6-C8	119.4	119.6990
C4-C6-H18	121.1	120.8084
C8-C6-H18	119.4	119.4926
C 4-C7-C10	120.1	120.0935
C 4-C7-H19	118.7	118.6707
C10-C7-H19	121.1	121.2358
C6-C8-C9	120.9	120.4914
C6-C8-C16	118.0	118.5478
C9-C8-C16	121.0	120.9609
C8-C9-C10	118.7	118.6867
C8-C9-C17	121.7	121.5693
C10-C9-C17	119.4	119.7440
C7-C10-C9	120.6	120.8959
C7-C10-H20	120.0	120.0719
C9-C10-H20	119.2	119.0323
C5-C11-C13	119.0	118.9707
C5-C11-H21	119.6	119.6143
C13-C11-H21	121.2	121.4120
C5-C12-C14	119.0	118.9721
C 5-C12-H22	119.6	119.6124
C14-C12-H22	121.2	121.4126
C11-C13-C15	120.3	120.2689
C11-C13-H23	119.5	119.5803
C15-C13-H23	120.1	120.1506

Table 8.1 (Contd..)Bond lengths (in Å), bond angles (in degree) and dihedral angles (in degree) of the dye 4PPN

Parameters	HF/6-311++G(d,p)	B3LYP/6-311++G(d,p)
C12-C14-C15	120.3	120.2674
C12-C14-H24	119.5	119.5797
C15-C14-H24	120.1	120.1527
C13-C15-C14	119.8	119.978
C13-C15-H25	120.0	120.0089
C14-C15-H25	120.0	120.0121
Dihedral Angle (°)		
C5-O1-C4-C6	-0.0362	0.0133
C5-O1-C4-C7	179.9662	-179.9876
C4-O1-C5-C11	91.3854	91.6632
C4-O1-C5-C12	-91.3633	-91.7513
O1-C4-C6-C8	-179.9947	-180.0011
O1-C4-C6-H18	0.0047	-0.0038
C7-C4-C6-C8	0.0028	-0.0002
C7-C4-C6-H18	-179.9978	179.9971
O1-C4-C7-C10	179.9955	180.003
O1-C4-C7-H19	-0.0035	0.0037
C6-C4-C7-C10	-0.0022	0.0022
C6-C4-C7-H19	179.9988	-179.9972
O1-C5-C11-C13	177.6333	176.7791
O1-C5-C11-H21	-1.8763	-2.6059
C12-C5-C11-C13	0.4423	0.2773
C12-C5-C11-H21	-179.0674	-179.1078
O1-C5-C12-C14	-177.6334	-176.7794
O1-C5-C12-H22	1.8769	2.6065
C11-C5-C12-C14	-0.4423	-0.2773
C11-C5-C12-H22	179.0681	179.1087
C4-C6-C8-C9	-0.0016	-0.0032
C4-C6-C8-C16	179.9958	179.9935
H18-C6-C8-C9	179.999	179.9995

Table 8.1 (Contd..)Bond lengths (in Å), bond angles (in degree) and dihedral angles (in degree) of the dye 4PPN

Parameters	HF/6-311++G(d,p)	B3LYP/6-311++G(d,p)
Dihedral Angle (°)		
H18-C6-C8-C16	-0.0036	-0.0037
C4-C7-C10-C9	0.0004	-0.0008
C4-C7-C10-H20	180.0001	179.9993
H19-C7-C10-C9	-180.0007	179.9985
H19-C7-C10-H20	-0.001	-0.0014
C6-C8-C9-C10	-0.0002	0.0045
C6-C8-C9-C17	179.9976	180.002
C16-C8-C9-C10	-179.9975	-179.9921
C16-C8-C9-C17	0.0003	0.0053
C8-C9-C10-C7	0.0009	-0.0025
C8-C9-C10-H20	-179.9989	179.9974
C17-C9-C10-C7	-179.997	-180.0
C17-C9-C10-H20	0.0033	-0.0001
C5-C11-C13-C15	-0.0956	-0.001
C5-C11-C13-H23	-179.9084	-179.8365
H21-C11-C13-C15	179.4059	179.3726
H21-C11-C13-H23	-0.4069	-0.463
C5-C12-C14-C15	0.0956	0.0011
C5-C12-C14-H24	179.9082	179.8367
H22-C12-C14-C15	-179.4067	-179.3734
H22-C12-C14-H24	0.406	0.4622
C11-C13-C15-C14	-0.2411	-0.2687
C11-C13-C15-H25	-179.9366	-179.9195
H23-C13-C15-C14	179.5707	179.5659
H23-C13-C15-H25	-0.1248	-0.0849
C12-C14-C15-C13	0.2412	0.2686
C12-C14-C15-H25	179.9367	179.9194
H24-C14-C15-C13	-179.5705	-179.566
H24-C14-C15-H25	0.125	0.0848

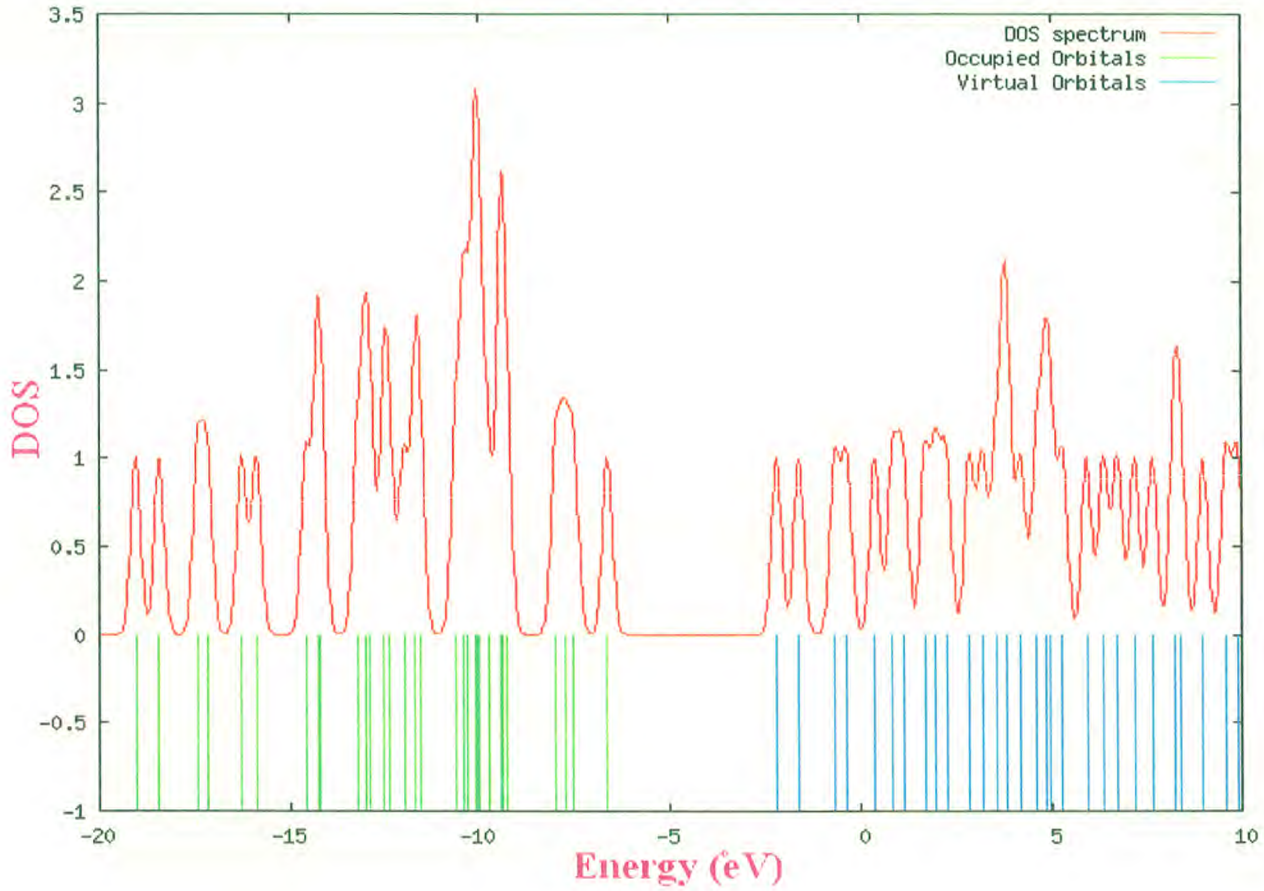

Figure 8.2 The frontier molecular orbital energies and corresponding density of state (DOS) spectrum of the dye 4PPN

corresponding density of state of the dye 4PPN is shown in Figure 8.2. The HOMO–LUMO gap of the dye 4PPN in vacuum is 4.59 eV.

While the calculated HOMO and LUMO energies of the bare $Ti_{38}O_{76}$ cluster as a model for nanocrystalline are -6.55 and -2.77eV, respectively, resulting in a HOMO–LUMO gap of 3.78 eV, the lowest transition is reduced to 3.20 eV according to TD-DFT, and this value is slightly smaller than typical band gap of TiO_2 nanoparticles with nm size [7]. Furthermore, the HOMO, LUMO and HOMO–LUMO gap of $(TiO_2)_{60}$ cluster is -7.52, -2.97, and 4.55 eV (B3LYP/VDZ), respectively [8]. Taking into account of the cluster size effects and the calculated HOMO, LUMO, HOMO–LUMO gap of the dye 4PPN, $Ti_{38}O_{76}$ and $(TiO_2)_{60}$ clusters, we can find that the HOMO energies of these dyes fall within the TiO_2 gap.

The above data also reveal the interfacial electron transfer between semiconductor TiO_2 electrode and the dye sensitizer 4PPN is electron injection processes from excited dye to the semiconductor conduction band. This is a kind of typical interfacial electron transfer reaction [9].

8.4.3 IR and Raman frequencies of 4PPN

Figure 8.3 and 8.4 shows the observed and calculated IR and Raman spectra of 4PPN respectively. Comparison of the observed (FT-IR and FT-Raman) and calculated vibrational frequencies of 4PPN is shown in Table 8.4. Comparison of the frequencies calculated by *ab initio* HF and B3LYP with experimental values reveals the overestimation of the calculated vibrational modes due to neglect of anharmonicity in real system. Inclusion of electron correlation in density functional theory to a certain extent makes the frequency values smaller in comparison with experimental values. Any way notwithstanding the level of calculations it is customary to scale down the calculated harmonic frequencies in order to improve the agreement with the experiment.

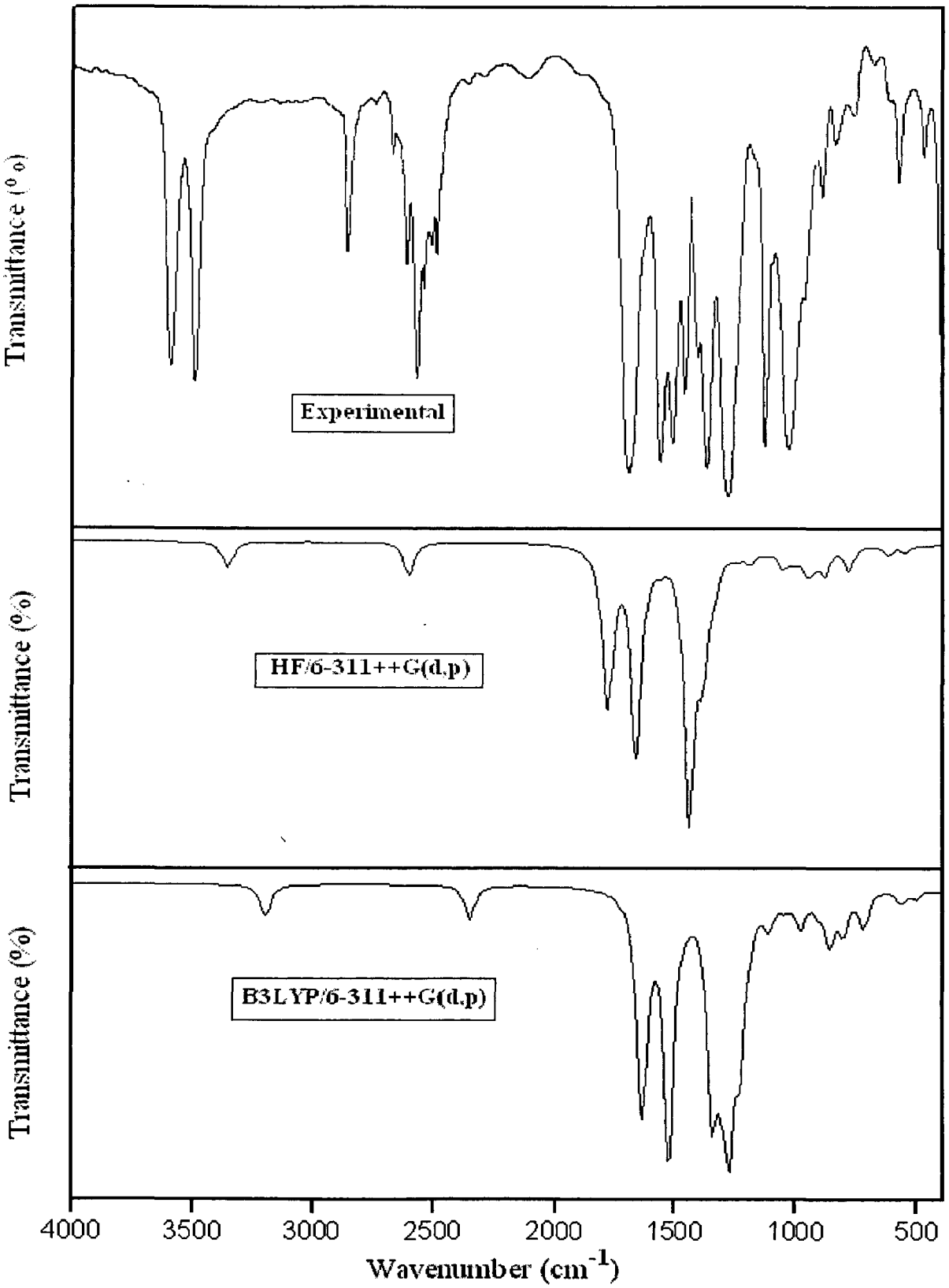

Figure 8.3 Observed and Calculated FT-IR Spectra of 4PPN

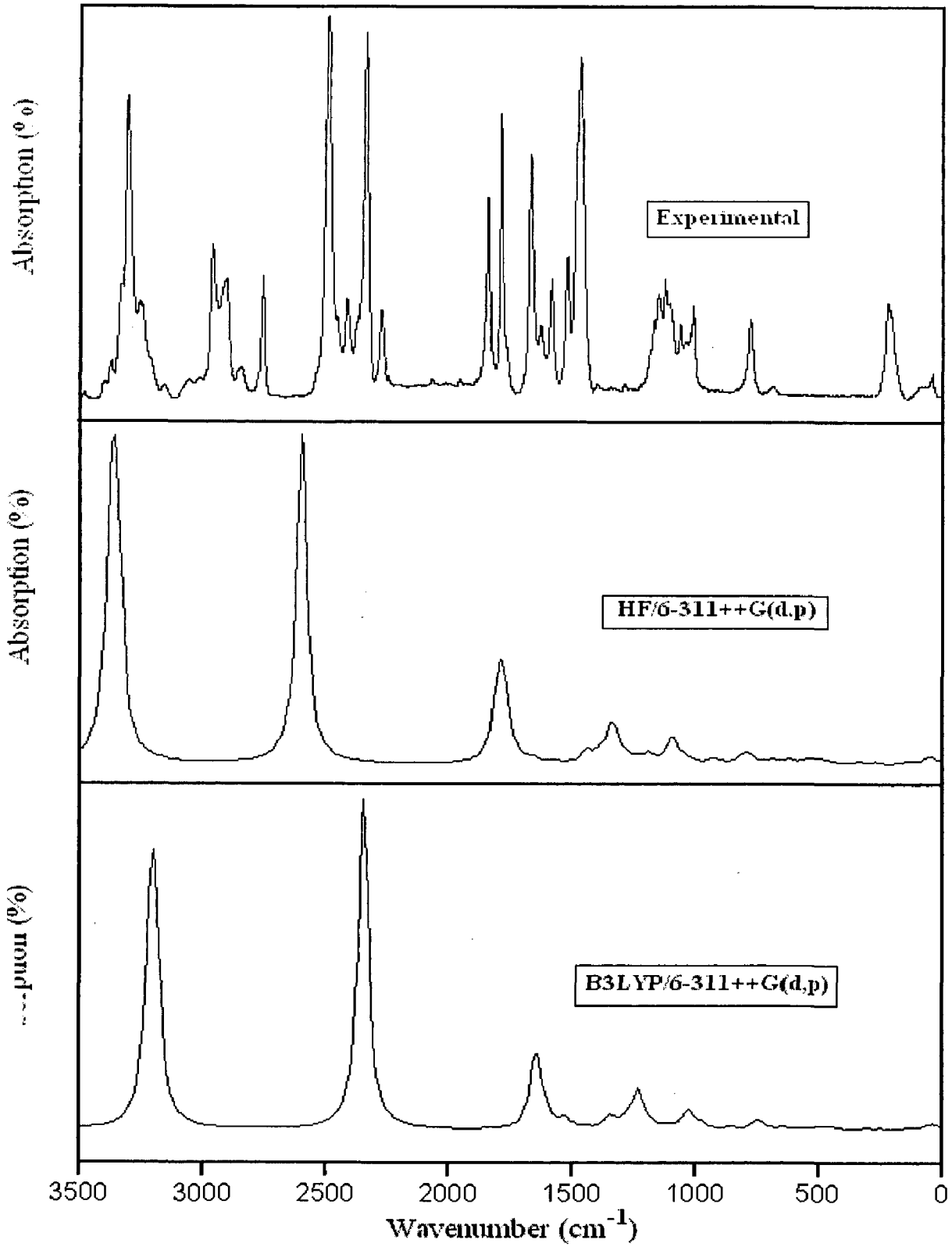

Figure 8.4 Observed and Calculated FT-Raman Spectra of 4PPN

Table 8.4 Comparison of the observed (FT-IR and FT-Raman) and calculated vibrational frequencies of 4PPN

Vibrational mode no	Species	Experimental Wavenumber (cm^{-1})		Scaled Wavenumber (cm^{-1})		IR Intensity (KM/ Mole)	Raman active (A^4/ AMU)	Assignments	PED (%)
		FT-IR	FT-Raman	HF/6-311++G (d,p)	B3LYP/6-311++G (d,p)				
1	A'	-	-	20	15	0.1	8.6	δ C-C	δ C-C (95)
2	A''	-	-	38	33	0.3	7.9	δ C-C	δ C-C (92)
3	A''	-	58	62	55	1.2	6.1	β-C-C-C	β-C-C-C (92)
4	A'	-	-	102	92	3.8	1.6	δ C-C	δ C-C (76)
5	A'	-	121	131	118	1.2	5.4	β C-C-N + β C-C-C	β C-C-N (71)+β C-C-C (23)
6	A'	-	-	157	143	2.5	0.7	δ C-C	δ C-C (82)
7	A'	-	-	174	159	4.9	0.8	β C-C-N	β C-C-N (89)
8	A'	-	254	265	242	0.6	4.2	β C-C-N	β C-C-N (90)
9	A'	-	-	276	251	0.9	0.1	δ C-C	δ C-C (93)
10	A''	-	312	327	303	1.8	5.5	β C-C-N + δ C-C	β C-C-N (55) + δ C-C(40)
11	A'	-	-	433	395	1.1	1.7	δ C-C	δ C-C (91)
12	A'	-	-	438	404	2.8	0.1	δ C-C	δ C-C(69)
13	A'	-	-	461	423	0.1	0.1	δ C-C	δ C-C (92)
14	A'	-	-	463	431	0.6	2.2	δ C-C	δ C-C (96)
15	A''	442	462	489	455	2.1	6.6	β C-C-N + δ C-C	β C-C-N(68)+ δ C-C (11)
16	A'	-	-	505	459	0.1	2.2	β C-H	β C-H (85)
17	A'	488	510	541	497	10.2	7.1	β C-C-N + δ C-C	β C-C-N (62) + δ C-C(30)
18	A'	560	562	609	555	13.8	4.5	δ C-C	δ C-C (94)

Table 8.4 (Contd..) Comparison of the observed (FT-IR and FT-Raman) and calculated vibrational frequencies of 4PPN

Vibrational mode no	Species	Experimental Wavenumber (cm^{-1})		Scaled Wavenumber (cm^{-1})		IR Intensity (KM/ Mole)	Raman active (A^4/ AMU)	Assignments	PED (%)
		FT-IR	FT-Raman	HF/6-311++G (d,p)	B3LYP/6-311++G (d,p)				
19	A'	-	-	610	559	1.1	0.9	β C-C-N + δ C-C	β C-C-N(58) + δ C-C (23)
20	A''	-	-	657	607	1.6	0.3	β C-C-N + δ C-C	β C-C-N (71) + δ C-C (28)
21	A''	-	641	673	629	0.1	4.8	δ C-C	δ C-C (98)
22	A'	-	-	698	641	0.3	1.4	δ C-C	δ C-C (99)
23	A'	-	-	705	649	0.4	1.1	β C-C-N + δ C-C	β C-C-N (64) + δ C-C (32)
24	A''	712	-	762	708	21.3	2.3	β C-C-N + δ C-C	β C-C-N (51)+ δ C-C (30)
25	A'	719	730	774	714	17.3	5.5	β C-C-N + δ C-C	β C-C-N (67) + δ C-C (22)
26	A'	-	762	790	741	1.4	21.4	β C-C-N + δ C-C + υ C-C	β C-C-N (39) + δ C-C (24) + υ C-C (18)
27	A''	-	-	811	746	0.1	1.2	δ C-C	δ C-C (90)
28	A''	822	-	872	796	40.1	0.4	δ C-C + γ C-H	δ C-C (78) + γ C-H (14)
29	A'	-	-	917	844	0.5	0.7	δ C-C + γ C-H	δ C-C (57) + γ C-H(34)
30	A'	862	897	940	850	21.1	6.6	υ C-O + δ C-C	υ C-O (44) + δ C-C (37)
31	A'	868	-	947	854	30.6	0.6	ω C-H	ω C-H (93)
32	A'	907	-	996	897	13.6	0.3	ω C-H	ω C-H(79)
33	A''	-	-	1026	930	2.8	1.3	ω C-H	ω C-H(93)
34	A''	981	1009	1048	973	34.4	13.1	δ C-C + υ C-C	δ C-C (60) + υ C-C (23)
35	A'	-	-	1085	981	0.1	0.3	δ C-C	δ C-C (97)
36	A'	-	-	1094	981	0.3	0.2	δ C-C	δ C-C (92)

Table 8.4 (Contd..) Comparison of the observed (FT-IR and FT-Raman) and calculated vibrational frequencies of 4PPN

Vibrational mode no	Species	Experimental Wavenumber (cm^{-1})		Scaled Wavenumber (cm^{-1})		IR Intensity (KM/ Mole)	Raman active (A^4/ AMU)	Assignments	PED (%)
		FT-IR	FT-Raman	HF/6-311++G (d,p)	B3LYP/6-311++G (d,p)				
37	A'	-	-	1099	1006	0.1	0.2	τ C-H	τ C-H (74)
38	A'	1031	1034	1114	1019	5.1	44.2	δ C-C	δ C-C (76)
39	A''	1083	1090	1118	1042	9.2	8.3	ω C-H	ω C-H(79)
40	A'	1138	-	1158	1094	7.2	0.6	δ C-C + ω C-H	δ C-C (48) + ω C-H (33)
41	A'	1154	1135	1181	1107	24.9	7.8	δ C-C + ω C-H	δ C-C (53) + ω C-H (32)
42	A'	-	1189	1197	1176	1.8	5.3	δ C-C + ω C-H	δ C-C (81) + ω C-H (11)
43	A'	-	-	1233	1182	0.1	3.0	ω C-H	ω C-H (95)
44	A'	1205	1196	1269	1187	14.7	5.3	υ C-C + ω C-H	υ C-C (66) + ω C-H (28)
45	A''	1241	1246	1281	1219	39.2	9.1	υ C-C + ω C-H + υ C-C-N	υ C-C (32) + ω C-H (25) + υ C-C-N (17)
46	A''	1236	1270	1313	1225	99.6	91.2	υ C-C + ω C-H + υ C-C-N	υ C-C (30) + ω C-H (49) + υ C-C-N(10)
47	A''	1279	1284	1319	1268	206.7	22.6	υ C-C + ω C-H + υ C-C-N	υ C-C (47) + ω C-H (23) + υ C-C-N (13)
48	A'	1321	-	1336	1302	100.1	3.9	υ C-C + ω C-H	υ C-C (56)+ ω C-H (34)
49	A'	-	-	1381	1322	0.6	0.3	ω C-H	ω C-H (99)
50	A''	1380	1364	1436	1340	194.3	31.3	υ_{asy} C=C	υ_{asy} C=C (98)
51	A'	-	-	1446	1344	0.1	1.3	ω C-H	ω C-H(80)
52	A'	1465	1498	1558	1441	8.3	6.4	υ_{sym} C=C + ω C-H	υ_{sym} C=C (58)+ ω C-H (33)

Table 8.4 (Contd..) Comparison of the observed (FT-IR and FT-Raman) and calculated vibrational frequencies of 4PPN

Vibrational mode no	Species	Experimental Wavenumber (cm^{-1})		Scaled Wavenumber (cm^{-1})		IR Intensity (KM/ Mole)	Raman active (A^4/ AMU)	Assignments	PED (%)
		FT-IR	FT-Raman	HF/6-311++G (d,p)	B3LYP/6-311++G (d,p)				
53	A'	-	-	1602	1485	3.4	1.6	ω C-H	ω C-H (92)
54	A'	1544	1534	1651	1518	225.1	5.7	υ_{sym} C-C-N + ω C-H	υ_{sym} C-C-N (64) + ω C-H(32)
55	A'	1562	1556	1661	1524	48.5	18.0	υ_{asy} C=C + ω C-H	υ_{asy} C=C (45) + ω C-H (39)
56	A'	1608	1615	1751	1595	14.8	21.4	υ_{asy} C=C + ω C-H	υ_{asy} C=C (55) + ω C-H (34)
57	A''	1635	1633	1775	1627	187.0	76.9	υ_{asy} C=C + ω C-H	υ_{asy} C=C (47) + ω C-H (24)
58	A'	1641	1645	1779	1636	6.5	7.8	ω C-H	ω C-H (99)
59	A''	1658	1657	1795	1644	43.4	135.2	υ_{asy} C=C + ω C-H	υ_{asy} C=C (79)+ ω C-H (12)
60	A'	2374	2378	2592	2339	29.1	655.5	υ_{sym} C-C-N	υ_{sym} C-C-N(99)
61	A'	2398	2391	2599	2345	6.5	248.8	υ_{asy} C-C-N	υ_{asy} C-C-N (97)
62	A'	3211	3207	3327	3172	0.5	36.7	υ_{sym} C-H	υ_{sym} C-H(93)
63	A'	3219	3216	3337	3180	5.1	135.9	υ_{asy} C-H	υ_{asy} C-H(87)
64	A'	3228	3224	3347	3189	15.9	73.5	υ_{asy} C-H	υ_{asy} C-H (96)
65	A'	3238	3235	3355	3196	7.2	4.4	υ_{asy} C-H	υ_{asy} C-H (95)
66	A'	3240	3241	3357	3196	1.0	60.5	υ_{sym} C-H	υ_{sym} C-H (94)
67	A''	3247	3265	3360	3200	3.5	339.5	υ_{sym} C-H	υ_{sym} C-H (94)
68	A'	3259	3289	3373	3209	0.4	178.3	υ_{sym} C-H	υ_{sym} C-H (99)
69	A'	3271	3314	3389	3221	0.9	63.5	υ CH	υ C-H (91)

υ - stretching; υ_{sym}-symmetric stretching ; υ_{asy}-asymmetric stretching; β-in plane bending; γ- out-of-plane bending; ω-wagging; τ- torsion ;

δ- Ring deformation

In our study we have followed two different scaling factors B3LYP/6-311++G(d,p) and HF/6-311G++(d,p).

The 4PPN molecule gives rise to thirty C-C ring deformations at 15, 33, 92, 143, 251, 303, 395, 404, 423, 431, 455, 497, 555, 559, 607, 629, 641, 649, 708, 714, 741, 746, 796, 844, 973, 981, 1019, 1094, 1107 and 1176 cm^{-1}, two C-C-C inplane bending vibrations at 55 and 118 cm^{-1}, twelve C-C-N inplane bending vibrations at 118, 159, 242, 303, 455, 497, 559, 607, 649, 708, 714 and 741 cm^{-1}, twenty three CH wagging at 854, 897, 930, 1042, 1094, 1107, 1176, 1182, 1187, 1219, 1225, 1268, 1302, 1322, 1344, 1441, 1485, 1518, 1524, 1595,1627, 1636 and 1644 cm^{-1}, seven C=C stretching vibrations at 741, 973, 1187, 1219, 1225, 1268 and 1302 cm^{-1}, one C-H inplane bending vibration at 459 cm^{-1}, two C-H out- of- plane bending vibrations at 796 and 844 cm^{-1}, one CO stretching vibration at 850 cm^{-1}, one C-H torsion at 1006 cm^{-1}, three C-C-N stretching vibrations at 1219, 1225 and 1268 cm^{-1}, five C=C asymmetric stretching vibrations at 1340, 1524, 1595, 1627 and 1644 cm^{-1}, one C=C symmetric stretching vibration at 1441 cm^{-1} , two C-C-N symmetric stretching vibrations at 1518 and 2339 cm^{-1}, one C-C-N asymmetric stretching vibration at 2345 cm^{-1}, four C-H symmetric stretching vibrations at 3172, 3196, 3200 and 3209 cm^{-1} , three C-H asymmetric stretching vibrations at 3180, 3189 and 3196 cm^{-1} and one C-H stretching vibration at 3221 cm^{-1} were assigned to B3LYP/6-311G++ (d,p) scaling method.

The strongest IR absorption for 4PPN corresponds to the vibrational mode 54 near about 1518 cm^{-1}, which is corresponding to stretching mode of C=C bonds. The next stronger IR absorption is attributed to vibrational mode 47 near about 1268 cm^{-1}, corresponding to the stretching mode of C=C bonds and stretching of C-C-N bond. In the Raman spectrum, however, the strongest activity mode is the vibrational mode 60 near

about 2339 cm^{-1}, which is corresponding to stretching mode of C-N triple bond. The same vibrations computed by HF/6-311++G(d,p) and also shows good agreement with experimental data.

8.4.4 Polarizability and hyperpolarizability of 4PPN

Polarizabilities and hyperpolarizabilities characterize the response of a system in an applied electric field [10]. They determine not only the strength of molecular interactions (long-range intermolecular induction, dispersion forces, etc.) as well as the cross sections of different scattering and collision processes, but also the nonlinear optical properties (NLO) of the system [11,12]. It has been found that the dye sensitizer hemicyanine system, which has high NLO property, usually possesses high photoelectric conversion performance [13]. In order to investigate the relationships among photocurrent generation, molecular structures and NLO, the polarizabilities and hyperpolarizabilities of 4PPN was calculated. Here, the polarizability and the first hyperpolarizabilities are computed using B3LYP/6-31G(d,p). The definitions [11,12] for the isotropic polarizability is

$$\alpha = \frac{1}{3}(\alpha_{XX} + \alpha_{YY} + \alpha_{ZZ}) \tag{8.1}$$

The polarizability anisotropy invariant is

$$\Delta\alpha = \left[\frac{(\alpha_{XX} - \alpha_{YY})^2 + (\alpha_{YY} - \alpha_{ZZ})^2 + (\alpha_{ZZ} - \alpha_{XX})^2}{2}\right]^{\frac{1}{2}} \tag{8.2}$$

and the average hyperpolarizability is

$$\beta_{ii} = \frac{1}{5}\sum_i(\beta_{iiZ} + \beta_{iZi} + \beta_{Zii}) \tag{8.3}$$

where, α_{XX}, α_{YY}, and α_{ZZ} are tensor components of polarizability; β_{iiZ}, β_{iZi}, and β_{Zii} (i from X to Z) are tensor components of hyperpolarizability. Tables 8.2 and 8.3 list the values of the polarizabilities and hyperpolarizabilities of the dye 4PPN.

Table 8.2 Polarizability (α) of the dye 4PPN (in a.u.)

α_{xx}	α_{xy}	α_{yy}	α_{xz}	α_{yz}	α_{zz}	α	$\Delta\alpha$
303.5	-0.5	177.9	-0.02	0.07	87.2	189.5	188.1

Table 8.3 Hyperpolarizability (β) of the dye 4PPN (in a.u.)

β_{xxx}	β_{xxy}	β_{xyy}	β_{yyy}	β_{xxz}	β_{xyz}	β_{yyz}	β_{xzz}	β_{yzz}	β_{zzz}	β_{ii}
1896.9	-471.6	1.7	60.3	0.04	0.01	-0.006	94.5	-35.2	0.001	0.021

In addition to the individual tensor components of the polarizabilties and the first hyperpolarizabilities, the isotropic polarizability, polarizability anisotropy invariant and hyperpolarizability are also calculated. The calculated isotropic polarizability of 4PPN is 189.5 a.u. However, the calculated isotropic polarizability of JK16, JK17, dye 1, dye 2, D5, DST and DSS is 759.9, 1015.5, 694.7, 785.7, 510.6, 611.2 and 802.9 a.u., respectively [14,15]. The above data indicate that the donor-conjugate π bridge-acceptor (D-π-A) chain-like dyes have stronger response for external electric field. Whereas, for

dye sensitizers D5, DST, DSS, JK16, JK17, dye 1 and dye 2, on the basis of the published photo-to-current conversion efficiencies, the similarity and the difference of geometries, and the calculated isotropic polarizabilities, it is found that the longer the length of the conjugate bridge in similar dyes, the larger the polarizability of the dye molecule, and the lower the photo-to-current conversion efficiency. This may be due to the fact that the longer conjugate-π-bridge enlarged the delocalization of electrons, thus it enhanced the response of the external field, but the enlarged delocalization may be not favorable to generate charge separated state effectively. So it induces the lower photo-to-current conversion efficiency.

8.4.5 Electronic absorption spectra and sensitized mechanism of 4PPN

Electronic absorption spectra of 4PPN in vacuum and solvent were performed using TD-DFT(PBE1PBE)/6-311++G(d,p) calculations, and the results are shown in Figure 8.5. It is observed that the absorption in the visible region is much weaker than that in the UV region for 4PPN. The results of TD-DFT have an appreciable red-shift in vacuum and solvent, and the degree of red-shift in solvent is more significant than that in vacuum.

The discrepancy between vacuum and solvent effects in TD-DFT calculations may result from two aspects. The first aspect is smaller gap of materials which induces smaller excited energies. The other is solvent effects. Experimental measurements of electronic absorptions are usually performed in solution. Solvent, especially polar solvent, could affect the geometry and electronic structure as well as the properties of molecules through the long-range interaction between solute molecule and solvent molecule. For these reasons it is more difficult to make the TD-DFT calculation is consistent with quantitatively.

Though the discrepancy exists, the TD-DFT calculations are capable of describing

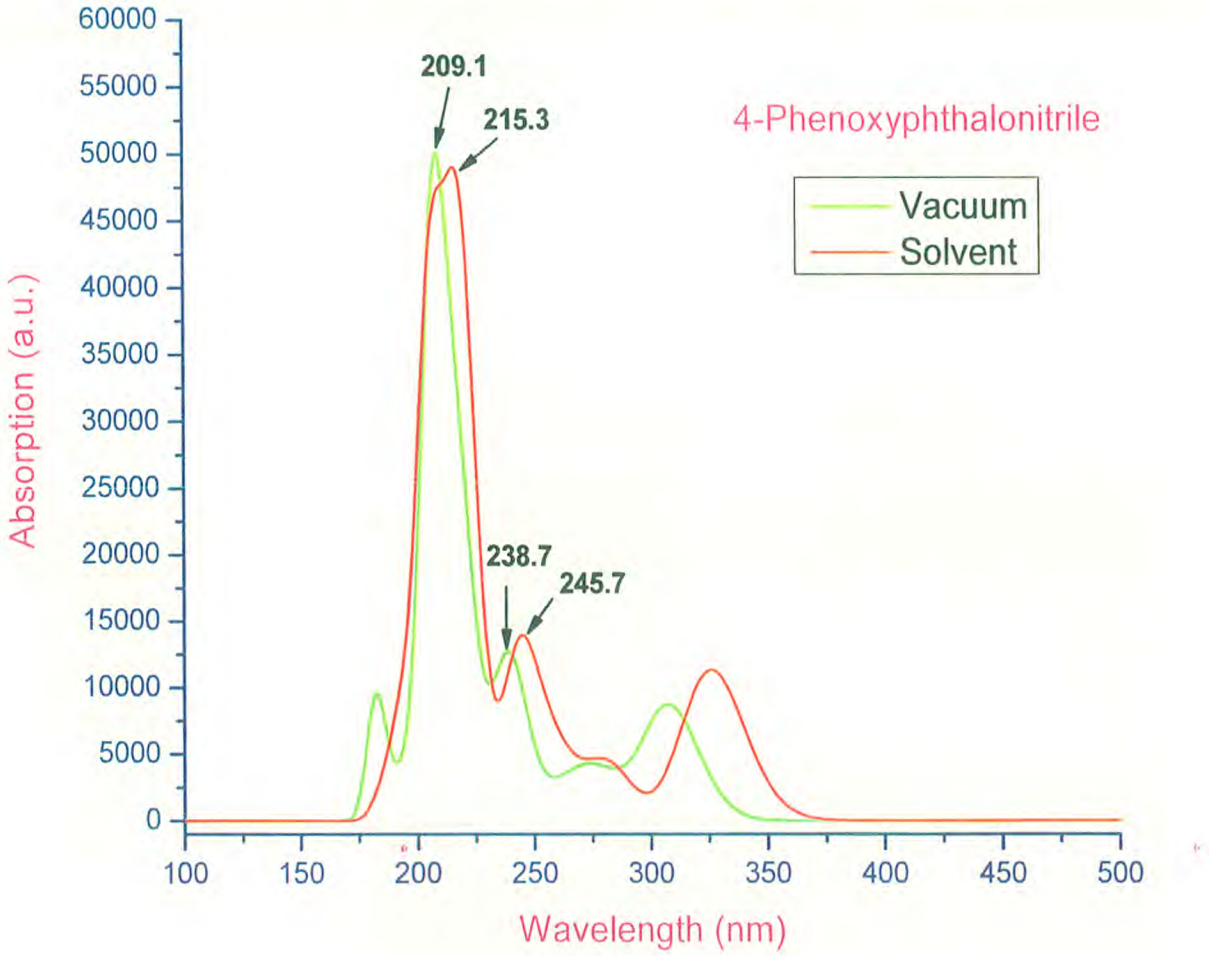

Figure 8.5 Calculated electronic absorption spectra of the dye 4PPN

the spectral features of 4PPN because of the agreement of lineshape and relative strength as compared with the vacuum and solvent.

The HOMO-LUMO gap of 4PPN in acetonitrile at PBE1PBE/6-311++G (d,p) theory level is smaller than that in vacuum. This fact indicates that the solvent effects stabilize the frontier orbitals of 4PPN. So it induces the smaller intensities and red-shift of the absorption as compared with that in vacuum. In order to obtain the microscopic information about the electronic transitions, the corresponding MO properties are checked. The absorption in visible and near-UV region is the most important region for photo-to-current conversion, so only the 20 lowest singlet/singlet transitions of the absorption band in visible and near-UV region for 4PPN is listed in Table 8.5. The data of Table 8.5 and Fig.8.6 are based on the 6-311++G (d,p) results with solvent effects involved. This indicates that the transitions are photoinduced charge transfer processes, thus the excitations generate charge separated states, which should favour the electron injection from the excited dye to semiconductor surface.

The solar energy to electricity conversion efficiency (η) under AM 1.5 white-light irradiation can be obtained from the following formula:

$$\eta(\%) = \frac{J_{SC}[mAcm^{-2}]V_{OC}[V]ff}{I_0[mWcm^{-2}]} \times 100 \qquad (8.4)$$

where I_0 is the photon flux, *Jsc* is the short-circuit photocurrent density, and *Voc* is the open-circuit photovoltage, and *ff* represents the fill factor [16]. At present, the *Jsc*, the *Voc*, and the *ff* are only obtained by experiment, the relationship among these quantities and the electronic structure of dye is still unknown. The analytical relationship between *Voc* and E_{LUMO} may exist. According to the sensitized mechanism (electron injected from the excited dyes to the semiconductor conduction band) and single electron and single state approximation, there is an energy relationship:

Table 8.5 Computed excitation energies, electronic transition configurations and oscillator strengths (f) for the optical transitions of the absorption bands in visible and near- UV region for the dye 4PPN in acetonitrile

State	Configurations composition (corresponding transition orbitals)	Excitation energy (eV/nm)	Oscillator strength (f)
1	0.68365 (57 → 58)	3.8065 / 325.72	0.1567
2	0.10446 (54 → 58) 0.50006 (56 → 58) -0.47544 (57 → 59)	4.3461 / 285.27	0.0020
3	0.49115 (56 → 58) 0.48174 (57 → 59)	4.4186 / 280.59	0.0569
4	-0.31756 (54 → 58) -0.16895 (54 → 59) 0.52316 (55 → 58) -0.25930 (55 → 59)	4.7770 /259.54	0.0622
5	-0.21618 (54 → 58) -0.22367 (55 → 58) -0.12427 (55 → 59) 0.59152 (56 → 59) -0.10712 (57 → 60)	5.0105 / 247.45	0.0228
6	0.35676 (54 → 58) 0.30876 (55 → 58) 0.33179 (55 → 59) 0.34177 (56 → 59)	5.0881 / 243.68	0.1538
7	0.14920 (56 → 59) -0.11342 (56 → 60) 0.34027 (56 → 61) 0.57540 (57 → 60) 0.11049 (57 → 61)	5.2940 / 234.20	0.0191
8	-0.28713 (54 → 58) 0.39265 (55 → 59) -0.11101 (56 → 60) -0.10158 (57 → 60) 0.40077 (57 → 61)	5.6653 / 218.85	0.5443
9	0.20717 (54→ 58) -0.29384 (55 → 59) -0.26362 (56 → 60) -0.13067 (57 → 60) 0.41253 (57 → 61) 0.16809 (57 →62)	5.9108 / 209.76	0.2561

Table 8.5 (Contd..) Computed excitation energies, electronic transition configurations and oscillator strengths (f) for the optical transitions of the absorption bands in visible and near- UV region for the dye 4 PPN in acetonitrile

State	Configurations composition (corresponding transition orbitals)	Excitation energy (eV/nm)	Oscillator strength (f)
10	0.10411 (53→ 58) 0.49855 (54 → 59) -0.14070 (55 → 60) -0.10846 (56 → 61) -0.32288 (57→ 62)	6.0547 / 204.77	0.2187
11	0.25758 (54→ 59) -0.17304 (55 →62) 0.16768 (56 → 60) 0.54611 (57 → 62)	6.0736 / 204.14	0.1478
12	-0.15741 (52 → 58) 0.55285 (53 → 58) -0.19808 (54 → 59) -0.21054 (55→60) -0.10730 (56 → 61)	6.2321 / 198.95	0.0436
13	0.10812 (49 → 58) 0.22684 (51→58) -0.25252 (52→ 58) 0.18261 (53→58) 0.13790 (54→59) 0.43416 (55→ 60) 0.20780 (56→ 61) -0.13786 (57→60) -0.12270 (57 → 61)	6.2799 / 197.43	0.0215
14	0.21900 (49→58) 0.35392 (51→58) -0.33622 (52→ 58) -0.32290 (53→ 58) -0.20452 (55→60) -0.10009 (56 → 61)	6.3114 / 196.44	0.0134
15	0.55827 (49→58) 0.18047 (50→58) -0.32012 (51→ 58) -0.10898 (51→ 59)	6.3578 / 195.01	0.0001

Table 8.5 (Contd..) Computed excitation energies, electronic transition configurations and oscillator strengths (f) for the optical transitions of the absorption bands in visible and near- UV region for the dye 4 PPN in acetonitrile

State	Configurations composition (corresponding transition orbitals)	Excitation energy (eV/nm)	Oscillator strength (f)
16	-0.11930 (55 → 60) 0.37922 (55 → 61) -0.11335 (55→62) 0.10334 (55 → 63) -0.34160 (56→60) -0.16842 (56→61) -0.33806 (57→ 63)	6.4560 / 192.05	0.0527
17	0.31846 (55→61) 0.18001 (55 → 62) -0.14658 (55→63) -0.15738 (56 → 60) 0.14035 (57 → 62) 0.49710 (57 →63)	6.4953 / 190.88	0.0265
18	-0.15119 (52 →58) 0.14823 (54 → 61) 0.34270 (54 → 62) 0.12730 (54 →63) 0.43677 (55 → 62) 0.13613 (55 → 63) -0.19421 (57 →63)	6.6793 / 185.63	0.0099
19	-0.11226 (46 → 58) -0.13036 (48 →58) 0.24378 (49 → 58) -0.16625 (50 → 58) 0.32911 (51 → 58) 0.44728 (52 → 58) 0.10786 (56 → 62)	6.7321 / 184.17	0.0047
20	-0.11805 (54→60) -0.11034 (55→ 60) -0.20126 (55→ 62) 0.13316 (56→61) 0.59139 (56 → 62) -0.10436 (57→ 62) 0.14179 (57→63)	6.7673 / 183.21	0.0138

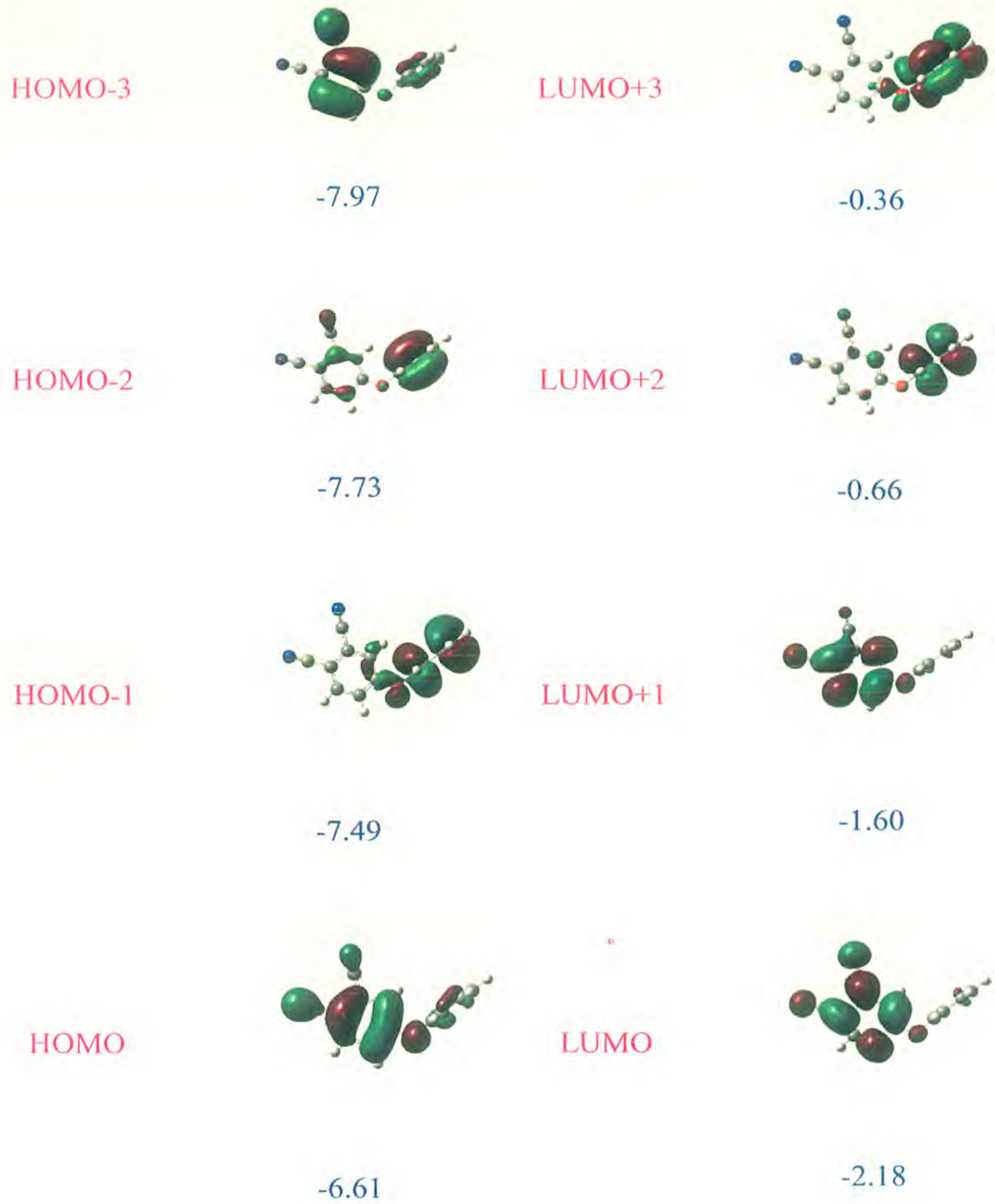

Figure 8.6 Isodensity plots (isodensity contour = 0.02 a.u.) of the frontier orbitals and orbital energies (in eV) of the dye 4PPN

$$eV_{oc} = E_{LUMO}\text{-}E_{CB} \tag{8.5}$$

where E_{CB} is the energy of the semiconductor's conduction band edge.

So the Voc may be obtained applying the following formula:

$$V_{oc} = \frac{(E_{LUMO}\text{-}E_{CB})}{e} \tag{8.6}$$

It induces that the higher the E_{LUMO}, the larger the V_{oc}. The results of organic dye sensitizer JK16 and JK17 [39], D-ST and D-SS also proved the tendency [17] (JK16: E_{LUMO} = -2.73 eV, V_{oc} = 0.74 V; JK17: E_{LUMO} = -2.87 eV, V_{oc} = 0.67 V; D-SS: E_{LUMO} = -2.91 eV, V_{oc} = 0.70 V; D-ST: E_{LUMO} = -2.83 eV, V_{oc} = 0.73 V). Certainly, this formula expects further test by experiment and theoretical calculation. The J_{sc} is determined by two processes, one is the rate of electron injection from the excited dyes to the conduction band of semiconductor, and the other is the rate of redox between the excited dyes and electrolyte. Electrolyte effect on the redox processes is very complex, and it is not taken into account in the present calculations. This indicates that most of excited states of 4PPN have larger absorption coefficient, and then with shorter lifetime for the excited states, so it results in the higher electron injection rate which leads to the larger Jsc of 4PPN. On the basis of above analysis, it is clear that the 4PPN has better performance in DSSC.

8.5. Conclusion

The geometries, electronic structures, polarizabilities, and hyperpolarizabilities of dye 4PPN was studied by using *ab initio* HF and density functional theory with hybrid functional B3LYP, and the UV-Vis spectra were investigated by using TDDFT methods. The NBO results suggest that 4PPN is a (D-π-A) system. The calculated isotropic

polarizability of 4PPN is 189.5 a.u and its calculated polarizability anisotropy invariant is 188.1 a.u. The hyperpolarizability of 4PPN is 0.021 a.u. The strongest IR absorption for 4PPN corresponds to the vibrational mode 54 near about 1518 cm^{-1}, which is corresponding to stretching mode of C=C bonds. In the Raman spectrum, the strongest activity mode is the vibrational mode 60 near about 2339 cm^{-1}, which is corresponding to stretching mode of C≡N bond. The electronic absorption spectral features in visible and near-UV region were assigned based on the qualitative agreement to TD-DFT calculations. The absorptions are all ascribed to $\pi \rightarrow \pi^*$ transition. The three excited states with the lowest excited energies of 4PPN is photoinduced electron transfer processes that contributes sensitization of photo-to-current conversion processes. The interfacial electron transfer between semiconductor TiO_2 electrode and dye sensitizer 4PPN is electron injection process from excited dye as donor to the semiconductor conduction band. Based on the analysis of geometries, electronic structures, and spectral properties of 4PPN the role of cyanine in phthalonitrile is as follows: it enlarged the distance between electron donor group and semiconductor surface, and decreased the timescale of the electron injection rate, resulted in giving lower conversion efficiency. This indicates that the choice of the appropriate conjugate bridge in dye sensitizer is very important to improve the performance of DSSC.

References :

[1] M.J. Frisch, G.W. Trucks, H.B. Schlegel, G.E. Scuseria, M.A. Robb, J.R. Cheeseman, J.A. Montgomery Jr., T. Vreven, K.N. Kudin, J.C. Burant, J.M. Millam, S.S. Iyengar, J. Tomasi, V. Barone, B. Mennucci, M. Cossi, G. Scalmani, N. Rega, G.A. Petersson, H. Nakatsuji, M. Hada, M. Ehara, K. Toyota, R. Fukuda, J. Hasegawa, M. Ishida, T. Nakajima, Y. Honda, O. Kitao, H. Nakai, M. Klene, X. Li, J.E. Knox, H.P. Hratchian, J.B. Cross, C. Adamo, J. Jaramillo, R. Gomperts, R.E. Stratmann, O. Yazyev, A.J. Austin, R. Cammi, C. Pomelli, J.W. Ochterski, P.Y. Ayala, K. Morokuma, G.A. Voth, P. Salvador, J.J. Dannenberg, V.G. Zakrzewski, S.Dapprich, A.D. Daniels, M.C. Strain, O. Farkas, D.K. Malick, A.D. Rabuck, K. Raghavachari, J.B. Foresman, J.V. Ortiz, Q. Cui, A.G. Baboul, S. Clifford, J.Cioslowski, B.B. Stefanov, G. Liu, A. Liashenko, P. Piskorz, I. Komaromi, R.L. Martin, D.J. Fox, T. Keith, M.A. Al-Laham, C.Y. Peng, A. Nanayakkara, M. Challacombe, P.M.W. Gill, B. Johnson, W. Chen, M.W. Wong, C. Gonzalez, J.A. Pople, Gaussian 03, Gaussian, Inc., Pittsburgh, PA, 2003.

[2] A.D. Becke, J. Chem. Phys. 98 (1993) 5648-5652.

[3] B. Miehlich, A. Savin, H. Stoll, H. Preuss, Chem. Phys. Lett. 157 (1989 200-206.

[4] C. Lee, W. Yang, R.G. Parr, Phys. Rev. B. 37 (1988) 785-789.

[5] V. Barone, M. Cossi, J. Phys. Chem. A 102 (1998) 1995-2001.

[6] M. Cossi, N. Rega, G. Scalmani, V. Barone, J. Comput. Chem. 24 (2003) 669-681.

[7] M.K. Nazeeruddin, F. De Angelis, S. Fantacci, A. Selloni, G. Viscardi, P. Liska, S.Ito, B. Takeru, M. Gratzel, J. Am. Chem. Soc. 127 (2005) 16835-16847.

[8] M.J. Lundqvist, M. Nilsing, P. Persson, S. Lunell, Int. J. Quantum Chem. 106 (2006) 3214-3234.

[9] D.F. Waston, G.J. Meyer, Annu. Rev. Phys. Chem. 56 (2005) 119-156.

[10] C. R. Zhang, H. S. Chen, and G. H. Wang, Chem. Res. Chin. U. 20 (2004) 640-646.

[11] Y. Sun, X. Chen, L. Sun, X. Guo, W. Lu, Chem.Phys. Lett. 381 (2003) 397-403.

[12] O. Christiansen, J. Gauss, J. F. Stanton, Chem.Phys. Lett. 305 (1999) 147-155.

[13] Z. S. Wang, Y. Y. Huang, C. H. Huang, J. Zheng, H.M. Cheng, S. J. Tian, Synth. Met. 14 (2000) 201-207.

[14] C.R. Zhang, Y.Z. Wu, Y.H. Chen, H.S. Chen, Acta Phys. Chim. Sin. 25 (2009) 53-60.

[15] A. Seidl, A. Gorling, P. Vogl, J. A. Majewski, M. Levy, Phys. Rev. B 53 (1996) 3764-3774.

[16] K. Hara, T. Sato, R. Katoh, A. Furube, Y. Ohga, A. Shinpo, S. Suga, K. Sayama, H.Sugihara, H. Arakawa, J. Phys. Chem. B. 107 (2003) 597-606.

[17] C.R. Zhang, Z.J. Liu, Y.H. Chen, H.S. Chen, Y.Z. Wu, L.H. Yuan, J. Mol. Struct. 899 (2009) 86-93.